communications materials

Article

https://doi.org/10.1038/s43246-024-00501-8

Isolated flat band in artificially designed Lieb lattice based on macrocycle supramolecular crystal

Cheng-Yi Chen[1], En Li[1], Huilin Xie[2], Jianyu Zhang[2], Jacky Wing Yip Lam[2], Ben Zhong Tang[2,3] & Nian Lin[1]

Isolated flat bands are known to host various strongly correlated phases due to the enhanced Coulomb interactions when the flat bands are gapped from dispersive bands. One way to achieve an isolated flat band is by breaking the on-site energy symmetry in a Lieb lattice. In this study, we demonstrate the design of such a Lieb lattice. The self-assembly of square-shaped macrocycle molecules on a Ag(111) surface forms a two-dimensional supramolecular crystal, comprising three types of nanopores with different sizes arranged in a Lieb lattice. The surface-state electrons of the Ag(111) substrate confined by these nanopores behave as quantum dots with specific energies depending on the pore size. Using scanning tunneling spectroscopy and plane-wave quantum simulation, we reveal that this artificial Lieb lattice exhibits an isolated flat band gapped at 0.16 eV from the nearest band. The supramolecular crystal is nearly defect-free and extends to sub-micrometer size, making it a practical platform for exploring the exotic properties of the isolated flat band.

In a flat band, the kinetic energy of electrons is suppressed, and electron-electron interactions dominate[1]. This leads to the emergence of strongly correlated phenomena, including ferromagnetism[2], Wigner crystals[3], superconductivity[4,5], superfluidity[6], Mott-Hubbard insulators[7], and fractional quantum Hall states[8–10]. The study of flat band physics using platforms of artificial systems has recently gained significant attentions[11,12]. The artificial systems include cold atoms[13–15], photonic crystals[16,17], quantum dot lattices[18], and molecular design[19,20]. Molecular design has been realized by means of tip manipulation of atoms or molecules[21–27] and molecular self-assembly[28–39]. Both approaches yield two-dimensional (2D) lattices of nanopores on noble metal surfaces, in which the nanopore potential wells confine the surface-state electrons of the underlying substrates, creating quantum dot (QD) arrays. Flat bands have been demonstrated in QD arrays arranged in a Kagome or Lieb lattice[23,24,38,39], but these flat bands intersect or contact dispersive bands, which compromises the Coulomb interaction. In order to enhance Coulomb interaction, isolated flat bands that do not intersect or contact dispersive bands are sought after[40–43]. In this work, we design an artificial Lieb lattice with an isolated flat band through breaking the symmetry of on-site energy of the lattice.

Results and discussion

Figure 1 illustrates the design principle. Figure 1a–c depict the band structures of the tight-binding (TB) model of a Lieb lattice (illustrated on the left) with different on-site energies. When the on-site energies of the three sites are equal, a flat band is crossed by a Dirac cone at the M point. Note that the flat band is not perfectly flat due to the non-zero next-nearest-neighbor interaction t_2. Figure 1b shows that breaking the on-site energy symmetry, i.e., reducing the corner site energy ε_2, separates the Dirac cone and opens a gap between the flat band and the lower band. Further breaking the symmetry by enlarging the on-site energy of the vertical-edge sites ε_1, as shown in Fig. 1c, opens a gap between the flat band and the upper band, resulting in an isolated flat band. To simulate the three TB models, we design three nanopore QD lattices as shown in Fig. 1d–f. By adjusting the size of the nanopores, the on-site energies of the QDs can be modified: smaller nanopores correspond to higher QD on-site energy. Figure 1g–i present the corresponding band structures of the three nanopore QD lattices calculated using a plane-wave (PW) method of muffin-tin potential. The QD lattices accurately reproduce the band structures of the TB models. Notably, the structure in Fig. 1f, comprising three different-sized nanopores, exhibits an

[1]Department of Physics, The Hong Kong University of Science and Technology, Clear Water Bay, Hong Kong, China. [2]Department of Chemistry and the Hong Kong Branch of Chinese National Engineering Research Center for Tissue Restoration and Reconstruction, The Hong Kong University of Science and Technology, Clear Water Bay, Hong Kong, China. [3]School of Science and Engineering, Shenzhen Institute of Aggregate Science and Technology, The Chinese University of Hong Kong, Shenzhen (CUHK-Shenzhen), Guangdong 518172, China. e-mail: phnlin@ust.hk

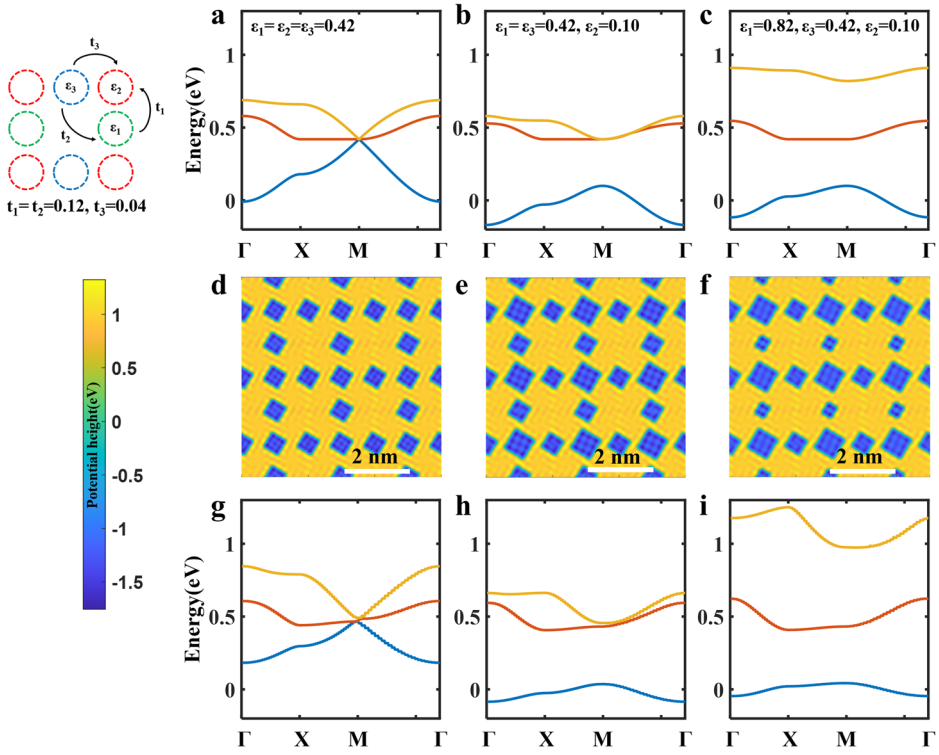

Fig. 1 | Design a Lieb lattice exhibiting an isolated flat band. a–c Tight-binding model (shown at left) band structures with the indicated on-site energies ($\varepsilon_{1,2,3}$) and hopping parameters ($t_{1,2,3}$), the red, blue, and green circles represent corner sites, horizontal-edge sites, and vertical-edge sites, respectively. **d–f** Nanopore QD lattices of different pore sizes. **g–i** Plane-wave calculation obtained band structures of the QD lattices of **d–f** respectively.

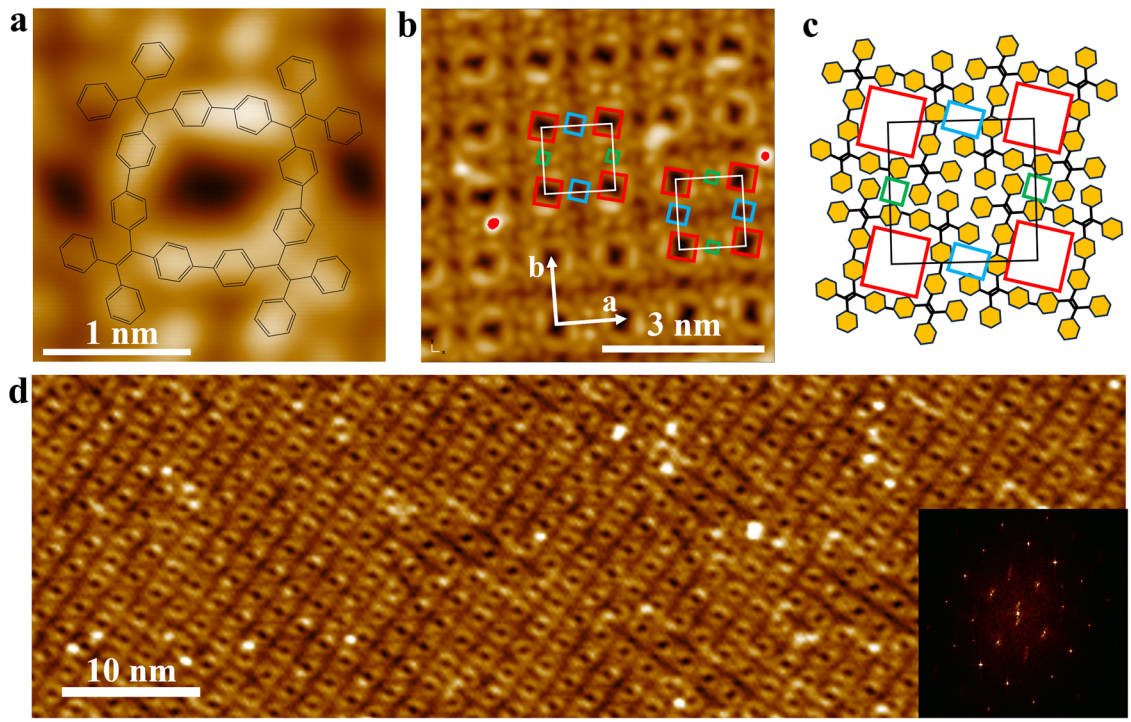

Fig. 2 | 2D supramolecular crystal of macrocycles. a High resolution STM topography ($V = -1.0$ V, $I = 150$ pA) of the macrocycle molecule with its chemical model overlaid. **b** STM topography ($V = -1$ V, $I = 100$ pA) showing the closely packed macrocycle molecules. The red, blue, and green squares mark the corner, the horizontal-edge and the vertical-edge sites of the artificial Lieb lattice, respectively. **c** The structure model of the 2D supramolecular crystal, where the red, blue, and green squares represent the intra- and inter-molecular nanopores. **d** Large-scale STM topography ($V = -1.0$ V, $I = 10$ pA) and the Fourie transformation (insert) showing the high crystallinity of the 2D supramolecular crystal.

isolated flat band. Since next-nearest-neighbor interactions are always present in the QD arrays, the flat band is not perfectly flat[23,24,39].

Experimentally, we utilize molecular self-assembly of square-shaped macrocycle molecules on an Ag(111) surface to create an artificial Lieb lattice[44]. Figure 2a displays a high-resolution scanning tunneling spectroscopy (STM) topography of a macrocycle with a chemical structure overlaid. The chemical structure has a 1 nm x 1 nm square cavity. However, the STM depicts a rectangular nanopore measuring 0.8 nm x 0.4 nm. Presumably,

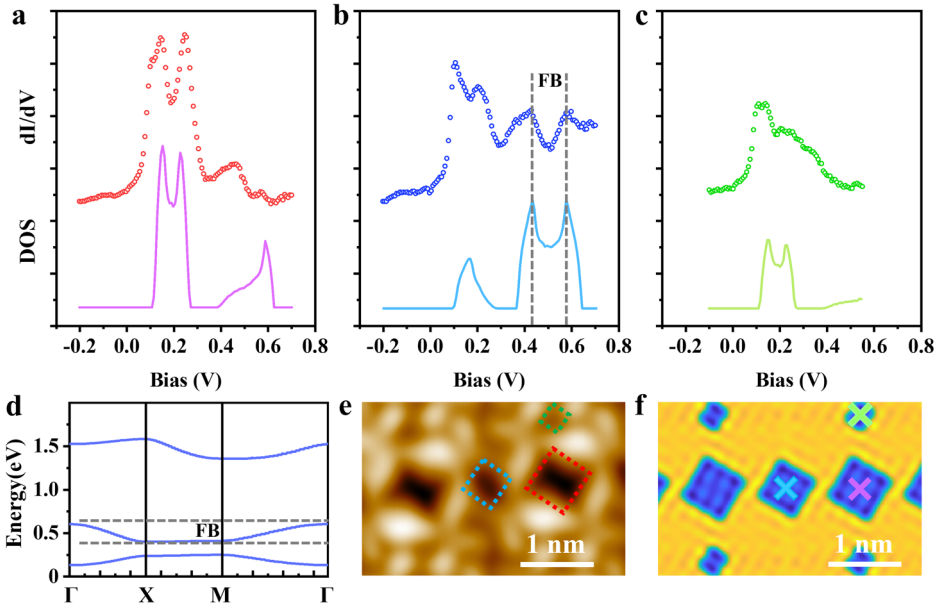

Fig. 3 | Electronic band structure of the artificial Lieb lattice. a–c Upper and lower spectra: site-specific *dI/dV* spectra (V_{mod} = 5 mV) and PW-calculated LDOS acquired at the corner site (**a**), the horizontal-edge site (**b**), and the vertical-edge site (**c**) of the Lieb lattice. **d** PW-calculated band structure of the QD Lieb lattice shown in (**f**). **e**, **f** STM topography (V = −0.4 V, I = 200 pA) and the QD artificial Lieb lattice structure, the squares and crosses mark the acquisition locations of the spectra in **a–c** with corresponding color.

different conformational orientations of the phenyl rings of the vertical and horizontal edges of the macrocycle skeleton determine the rectangular shape of the nanopore. Figure 2b shows that the macrocycle molecules form a closely packed 2D supramolecular crystal with a four-fold symmetry. Careful inspections reveal that the lattice is slightly elongated (4%) in one direction (**a** = 2.01 ± 0.02 nm, **b** = 2.06 ± 0.03 nm). We attribute this deviation from a perfect square lattice to the symmetry mismatch between the four-fold 2D molecular crystal and the three-fold Ag(111) substrate lattice. Figure 2c presents a tentative model of the 2D supramolecular crystal, suggesting that the exterior phenyl groups of the adjacent macrocycle molecules interact through π-π interactions.

In the 2D supramolecular crystal, the macrocycle cavities provide intra-molecular nanopores (highlighted in red squares), while the voids between neighboring macrocycles create inter-molecular nanopores (highlighted in blue and green squares in Fig. 2c). Due to the rectangular lattice, the inter-molecular nanopores at the horizontal-edges (blue squares) are larger than those at the vertical-edges (green squares). The size difference of the inter-molecular nanopores along the two orthogonal directions is apparent in Fig. 2b, which displays two rectangular lattices with a 90° rotation. The organic skeleton of the macrocycles consists of phenyl rings, which are known to repel surface-state electrons[45–48]. Consequently, the nanopores confine surface-state electrons, acting as QDs. The arrangement of nanopores in this structure resembles the Lieb lattice shown in Fig. 1f. Specifically, the intra-molecular nanopores marked by red squares represent the corner site QDs, while the inter-molecular nanopores marked by blue and green squares represent the larger and smaller edge site QDs, respectively. Large-scale STM imaging demonstrates that the 2D supramolecular crystal is nearly defect-free, as depicted in Fig. 2d. A Fourier transformation of Fig. 2d, displayed in the inset, reveals sharp spots, indicating the 2D supramolecular crystal has exceptionally high crystallinity. The single domains of the 2D supramolecular crystal can extend to sub-micrometer size (For large-scale STM topography of 2D supramolecular crystal showing high crystallinity and big domain size see Supplementary Fig. 1).

To investigate the electronic structure of the artificial Lieb lattice, we conduct site-specific differential tunneling conductance (*dI/dV*) measurements to reveal the local density of states (LDOS). Figure 3a–c (upper spectra) depict the *dI/dV* spectra obtained at the centers of a corner site (marked by the red square in Fig. 3e), a horizontal-edge site (blue square), and a vertical-edge site (green square), correspondingly (For *dI/dV* spectra normalized by tip state see Supplementary Fig. 2). The corner site spectrum displays two prominent peaks at 0.15 and 0.25 V and two weaker peaks at 0.46 and 0.60 V. Interestingly, neighboring corner sites exhibit *dI/dV* spectra featuring similar two strong peaks but with different relative peak intensity (Supplementary Fig. 3). Uneven LDOS at neighboring quantum wells of an identical shape indicates that the LDOS peaks are not isolated quantum well states but rather associated with a dispersive band of the QD lattice. The horizontal-edge site spectrum (Fig. 3b) exhibits four peaks peaked at comparable energies (0.11, 0.21, 0.43, and 0.57 V). However, compared with the LDOS at the corner site, the intensity of the two low-energy peaks is reduced, while the two high-energy peaks become stronger. The spectrum of the vertical-edge site (Fig. 3c) displays a peak at 0.12 V and a downhill slope from 0.18 to 0.45 V. It is worthwhile to note that these rich LDOS features do not originate from the macrocycle molecules (Supplementary Fig. 4). Instead, we contend that they arise from the QD states of the nanopores.

Based on the structure resolved in the STM image (Fig. 3e), we construct a QD Lieb lattice model structure, as depicted in Fig. 3f. Figure 3d displays the band structure of this QD artificial Lieb lattice solved using PW calculation. Referring to Fig. 1, the lower and upper bands in Fig. 3d are assigned to the split Dirac cone bands. The middle band is the isolated flat band, which is separated from the lower and upper bands by a gap of 0.16 and 0.75 eV, respectively. The flat band is nearly perfectly flat from the X point to the M point. The band bending near the Γ point is due to the next-nearest-neighbor interaction, resulting in a bandwidth of 0.2 eV.

Figure 3a–c (lower spectra) depict the PW-calculated LDOS at the centers of the three potential wells. At the corner site (marked by the pink cross in Fig. 3f), the LDOS is present in two energy regions of 0.10 V–0.26 V and 0.40 V–0.62 V. In the first energy region, there are two strong LDOS peaks at 0.15 and 0.24 V, while in the second energy region, the LDOS displays a shoulder at 0.47 V and a weak peak at 0.60 V. At the horizontal-edge site (marked by the blue cross), the LDOS is present in the same two energy regions, but with different intensity which displays a weak peak at 0.16 V in the first energy region and two strong peaks at 0.43 and 0.58 V in the second energy region. At the vertical-edge site (marked by the green cross), the LDOS is mostly present in the first energy region with two peaks at 0.15 and 0.24 V. In comparison with the experimental data obtained at the equivalent sites, shown as the upper spectra in Fig. 3a–c, the LDOS of the QD Lieb lattice model structure captures the characteristics of the experimental *dI/dV* spectra. Specifically, the intensity of the peaks in the first/second energy region at the horizontal-edge site is reduced/enhanced compared to those at the corner site. The LDOS can be mapped to the band structure shown in Fig. 3d. Specifically, the LDOS in the first energy region

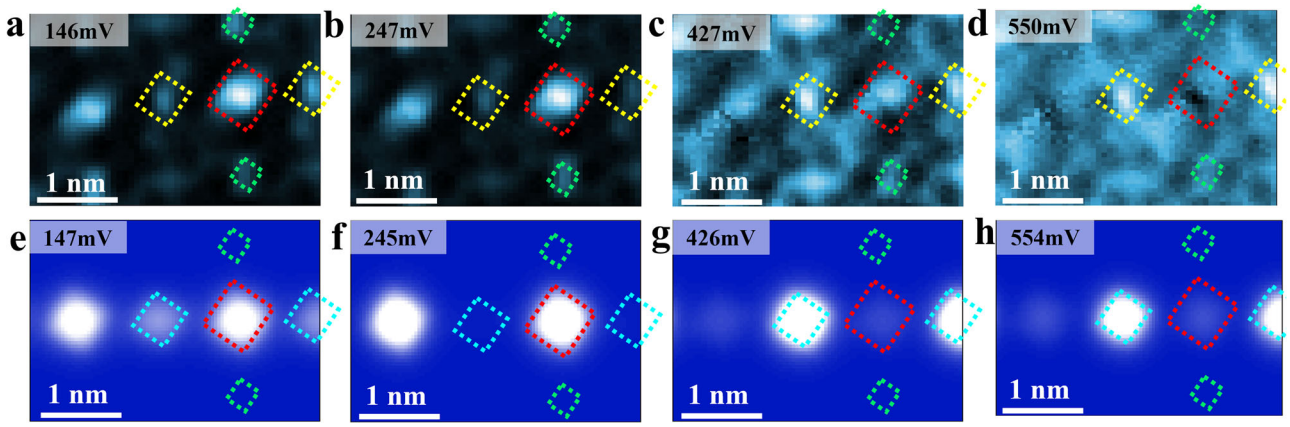

Fig. 4 | LDOS spatial distribution of the artificial Lieb lattice. a–d Spatially resolved *dI/dV* maps (V_{mod} = 7 mV) at the indicated energies. **e–h** PW-calculated LDOS distributions at the indicated energies. The positions of the corner, horizontal-edge and vertical-edge sites are marked with red, yellow/blue and green squares, respectively.

originates from the lower band, while the LDOS in the second energy region originates from the isolated flat band, where the flat part from the X point to the M point at the band bottom corresponds to the 0.43 V peak and the top part of the band corresponds to the 0.58 V peak.

To probe the spatial distribution of the bands, we acquire spatially resolved *dI/dV* maps at specific energies. As shown in Fig. 4a, b, the *dI/dV* signal at 146 and 247 mV is strongest at the corner sites (marked by the red squares). The horizontal-edge sites (marked by the yellow squares) display relatively weak intensity at the same energies. At 427 and 550 mV, as shown in Fig. 4c, d, the state intensity at the horizontal-edge site is enhanced and surpasses the intensity at the corner sites. The PW calculated spatial distributions of the density of states at the indicated energies confirm the energy-dependent intensity reversal at the corner and horizontal-edge sites, as depicted in Fig. 4e–h. The simulated spatial distributions of the density of states at other energies (Supplementary Fig. 5) also match the experimental data (Supplementary Fig. 6) very well. The energy-dependent LDOS spatial distributions can be mapped to the band structure (Fig. 3d): the states of the lower band (at 146 and 247 mV) are mostly distributed at the corner sites, while the states of the isolated flat band (at 426 and 554 mV) are predominantly distributed at the horizontal-edge sites[23,39]. To summarize, the observed LDOS localization of the isolated flat band at the horizontal-edge sites is an interference phenomenon of the surface electrons in the Lieb lattice.

Conclusions

In conclusion, we have successfully demonstrated the realization of an artificial Lieb lattice featuring an isolated flat band in a 2D supramolecular crystal of square-shaped macrocycles self-assembled on a Ag(111) surface. The intra- and inter-molecular nanopores in the 2D supramolecular crystal provide quantum dots arranged in a Lieb lattice with varying energy levels, which is the key factor in forming the isolated flat band. Compared with the structures built by tip manipulation of molecules[21–24], the ultra-large single domain size, high crystallinity, and thermal stability of this system make it an ideal platform for exploring the flat band physics, e.g., the correlated states and the possible topological nontrivial phases, using a wide range of techniques, such as various spectroscopic and transport experiments.

Methods

Sample preparation and measurement

4,4'-(2,2-diphenylethene-1,1-diyl)bis(bromobenzene) molecules are evaporated at 140 °C, with a deposition rate of ~0.66 ML h^{-1}, while the Ag(111) substrate is held at 200 °C. The slow deposition and hot substrate method allows for pseudo-high-dilution and improves the macrocycle yield. Subsequently, the on-surface synthesized macrocycles self-assemble as the 2D supramolecular crystal[44]. The sample is transferred to the STM chamber, where STM topography is acquired with constant current mode and scanning tunneling spectroscopy (STS) spectra are acquired at 5 K using the lock-in technique with a modulation frequency of 787.3 Hz. The STS spectra shown in Fig. 3 are not normalized by the spectra acquired on the clean surface.

Plane-wave calculation

The Shockley surface state of Ag(111) is modeled as a 2D electron gas (2DEG) with an effective electron mass ($m_{eff} = 0.42\ m_e$). The 2-dimensional time-independent Schrödinger equation can be expressed as:

$$-\frac{\hbar^2}{2m}\vec{\nabla}^2\psi(\vec{x}) + V_M(\vec{x})\psi(\vec{x}) = E\psi \quad (1)$$

where V_M represents the potential provided by the macrocycles. The wavefunction $\psi(\vec{x})$ is solved numerically using the Bloch's Theorem. The parameters of the QD lattice structure shown in Fig. 3f are the following: corner-site potential wells: 0.65 nm x 0.65 nm, horizontal-edge-site potential wells: 0.61 nm x 0.61 nm, vertical-edge-site potential wells: 0.27 nm x 0.37 nm, and potential well depth: 2.4 V (Supplementary Note 1).

Data availability

The data that support the plots within this article is available from the corresponding authors upon reasonable request.

Code availability

The computer codes that support the findings of this study are available from the corresponding author upon request.

Received: 4 January 2024; Accepted: 10 April 2024;
Published online: 16 April 2024

References

1. Liu, Z., Liu, F. & Wu, Y.-S. Exotic electronic states in the world of flat bands: from theory to material. *Chin. Phys. B* **23**, 077308 (2014).
2. Tasaki, H. From Nagaoka's ferromagnetism to flat-band ferromagnetism and beyond: an introduction to ferromagnetism in the Hubbard model. *Prog. Theor. Phys.* **99**, 489–548 (1998).
3. Wu, C., Bergman, D., Balents, L. & Sarma, S. D. Flat bands and Wigner crystallization in the honeycomb optical lattice. *Phys. Rev. Lett.* **99**, 070401 (2007).
4. Miyahara, S., Kusuta, S. & Furukawa, N. BCS theory on a flat band lattice. *Phys. C* **460**, 1145–1146 (2007).
5. Kopnin, N., Heikkilä, T. & Volovik, G. High-temperature surface superconductivity in topological flat-band systems. *Phys. Rev. B* **83**, 220503 (2011).

6. Julku, A., Peotta, S., Vanhala, T. I., Kim, D.-H. & Törmä, P. Geometric origin of superfluidity in the Lieb-lattice flat band. *Phys. Rev. Lett.* **117**, 045303 (2016).
7. Lieb, E. H. Two theorems on the Hubbard model. *Phys. Rev. Lett.* **62**, 1201–1204 (1989).
8. Bergholtz, E. J. & Liu, Z. Topological flat band models and fractional Chern insulators. *Int. J. Mod. Phys. B* **27**, 1330017 (2013).
9. Jaworowski, B., Manolescu, A. & Potasz, P. Fractional Chern insulator phase at the transition between checkerboard and lieb lattices. *Phys. Rev. B* **92**, 245119 (2015).
10. Tang, E., Mei, J.-W. & Wen, X.-G. High-temperature fractional quantum hall states. *Phys. Rev. Lett.* **106**, 236802 (2011).
11. Leykam, D., Andreanov, A. & Flach, S. Artificial flat band systems: from lattice models to experiments. *Adv. Phys. X* **3**, 1473052 (2018).
12. Polini, M., Guinea, F., Lewenstein, M., Manoharan, H. C. & Pellegrini, V. Artificial honeycomb lattices for electrons, atoms and photons. *Nat. Nanotechnol.* **8**, 625–633 (2013).
13. Shen, R., Shao, L., Wang, B. & Xing, D. Single Dirac cone with a flat band touching on line-centered-square optical lattices. *Phys. Rev. B* **81**, 041410 (2010).
14. Goldman, N., Urban, D. & Bercioux, D. Topological phases for fermionic cold atoms on the Lieb lattice. *Phy. Rev. A* **83**, 063601 (2011).
15. Apaja, V., Hyrkäs, M. & Manninen, M. Flat bands, Dirac cones, and atom dynamics in an optical lattice. *Phys. Rev. A* **82**, 041402 (2010).
16. Vicencio, R. A. et al. Observation of localized states in Lieb photonic lattices. *Phys. Rev. Lett.* **114**, 245503 (2015).
17. Mukherjee, S. et al. Observation of a localized flat-band state in a photonic lieb lattice. *Phys. Rev. Lett.* **114**, 245504 (2015).
18. Tamura, H., Shiraishi, K., Kimura, T. & Takayanagi, H. Flat-band ferromagnetism in quantum dot superlattices. *Phys. Rev. B* **65**, 085324 (2002).
19. Freeney, S. E., Slot, M. R., Gardenier, T. S., Swart, I. & Vanmaekelbergh, D. Electronic quantum materials simulated with artificial model lattices. *ACS Nanosci. Au* **2**, 198–224 (2022).
20. Piquero-Zulaica, I. et al. Engineering quantum states and electronic landscapes through surface molecular nanoarchitectures. *Rev. Mod. Phys.* **94**, 045008 (2022).
21. Gomes, K. K., Mar, W., Ko, W., Guinea, F. & Manoharan, H. C. Designer Dirac fermions and topological phases in molecular graphene. *Nature* **483**, 306–310 (2012).
22. Wang, S., Tan, L. Z., Wang, W., Louie, S. G. & Lin, N. Manipulation and characterization of aperiodical graphene structures created in a two-dimensional electron gas. *Phys. Rev. Lett.* **113**, 196803 (2014).
23. Slot, M. R. et al. Experimental realization and characterization of an electronic Lieb lattice. *Nat. Phys* **13**, 672–676 (2017).
24. Drost, R., Ojanen, T., Harju, A. & Liljeroth, P. Topological states in engineered atomic lattices. *Nat. Phys* **13**, 668–671 (2017).
25. Gardenier, T. S. et al. p orbital flat band and Dirac cone in the electronic honeycomb lattice. *ACS Nano.* **14**, 13638–13644 (2020).
26. Kempkes, S. et al. Robust zero-energy modes in an electronic higher-order topological insulator. *Nat. Mater.* **18**, 1292–1297 (2019).
27. Kempkes, S. N. et al. Design and characterization of electrons in a fractal geometry. *Nat. Phys.* **15**, 127–131 (2019).
28. Piquero-Zulaica, I. et al. Electron transmission through coordinating atoms embedded in metal-organic nanoporous networks. *Phys. Rev. Lett.* **123**, 266805 (2019).
29. Müller, K., Enache, M. & Stöhr, M. Confinement properties of 2D porous molecular networks on metal surfaces. *J. Phys. Condens. Matter.* **28**, 153003 (2016).
30. Klappenberger, F. et al. Tunable quantum dot arrays formed from self-assembled metal-organic networks. *Phys. Rev. Lett.* **106**, 026802 (2011).
31. Klappenberger, F. et al. Dichotomous array of chiral quantum corrals by a self-assembled nanoporous kagomé network. *Nano Lett.* **9**, 3509–3514 (2009).
32. Kawai, S. et al. Near fermi superatom state stabilized by surface state resonances in a multiporous molecular network. *Nano Lett.* **21**, 6456–6462 (2021).
33. Lobo-Checa, J. et al. Band formation from coupled quantum dots formed by a nanoporous network on a copper surface. *Science* **325**, 300–303 (2009).
34. Piquero-Zulaica, I. et al. Surface state tunable energy and mass renormalization from homothetic quantum dot arrays. *Nanoscale* **11**, 23132–23138 (2019).
35. Kepčija, N., Huang, T.-J., Klappenberger, F. & Barth, J. Quantum confinement in self-assembled two-dimensional nanoporous honeycomb networks at close-packed metal surfaces. *J. Chem. Phys.* **142**, 101931 (2015).
36. Wang, S. et al. Tuning two-dimensional band structure of Cu (111) surface-state electrons that interplay with artificial supramolecular architectures. *Phys. Rev. B* **88**, 245430 (2013).
37. Piquero-Zulaica, I. et al. Precise engineering of quantum dot array coupling through their barrier widths. *Nat. Commun.* **8**, 787 (2017).
38. Telychko, M. et al. Ultrahigh-yield on-surface synthesis and assembly of circumcoronene into a chiral electronic kagome-honeycomb lattice. *Sci. Adv.* **7**, eabf0269 (2021).
39. Qiu, W.-X., Li, S., Gao, J.-H., Zhou, Y. & Zhang, F.-C. Designing an artificial Lieb lattice on a metal surface. *Phys. Rev. B* **94**, 241409 (2016).
40. Huda, M. N., Kezilebieke, S. & Liljeroth, P. Designer flat bands in quasi-one-dimensional atomic lattices. *Phys. Rev. Res.* **2**, 043426 (2020).
41. Li, S., Xie, Y. & Chen, Y. Isolated flat bands in a lattice of interlocking circles. *Phys. Rev. B* **104**, 085127 (2021).
42. Wang, J. & Quek, S. Y. Isolated flat bands and physics of mixed dimensions in a 2D covalent organic framework. *Nanoscale* **12**, 20279–20286 (2020).
43. Green, D., Santos, L. & Chamon, C. Isolated flat bands and spin-1 conical bands in two-dimensional lattices. *Phys. Rev. B* **82**, 075104 (2010).
44. Li, E. et al. On-surface synthesis and spontaneous segregation of conjugated tetraphenylethylene macrocycles. *Commun. Chem.* **5**, 174 (2022).
45. Taber, B. N. et al. Quantum confinement of surface electrons by molecular nanohoop corrals. *J. Phys. Chem. Lett.* **7**, 3073–3077 (2016).
46. Gross, L. et al. Scattering of surface state electrons at large organic molecules. *Phys. Rev. Lett.* **93**, 056103 (2004).
47. Piquero-Zulaica, I. et al. Effective determination of surface potential landscapes from metal-organic nanoporous network overlayers. *New. J. Phys.* **21**, 053004 (2019).
48. Peng, X. et al. Visualizing designer quantum states in stable macrocycle quantum corrals. *Nat. Commun.* **12**, 5895 (2021).

Acknowledgements

This work is partially supported by the Research Grants Council of Hong Kong (Project 16301921), and the National Key R&D Program of China (2020YFA0309600).

Author contributions

N.L. conceived and supervised the work. C.C. and E.L. performed the STM/STS experiments; H.X. and J.Z. synthesized the precursor molecules under the supervision of J.W.Y.L. and B.Z.T.; C.C. analyzed the experimental data and performed calculation. C.C. and N.L. wrote the manuscript.

Competing interests

The authors declare no competing interests.

Additional information

Supplementary information The online version contains supplementary material available at https://doi.org/10.1038/s43246-024-00501-8.

Correspondence and requests for materials should be addressed to Nian Lin.

Peer review information *Communications Materials* thanks Daniel Multer and the other, anonymous, reviewer(s) for their contribution to the peer review of this work. Primary Handling Editor: Aldo Isidori. A peer review file is available.